Chinese Chemical Letters 36 (2025) 109925

Contents lists available at ScienceDirect

Chinese Chemical Letters

journal homepage: www.elsevier.com/locate/cclet

An overview of photothermal materials for solar-driven interfacial evaporation

Yiming Fang[a], Huimin Gao[a,*], Kaiting Cheng[a], Liang Bai[a], Zhengtong Li[b,*], Yadong Zhao[c], Xingtao Xu[a,*]

[a] Marine Science and Technology College, Zhejiang Ocean University, Zhoushan 316022, China
[b] State Key Laboratory of Hydrology-Water Resources and Hydraulic Engineering, Hohai University, Nanjing 210098, China
[c] School of Food and Pharmacy, Zhejiang Ocean University, Zhoushan 316022, China

ARTICLE INFO

Article history:
Received 24 October 2023
Revised 24 March 2024
Accepted 24 April 2024
Available online 25 April 2024

Keywords:
Solar-driven interfacial evaporation
Desalination
Wastewater treatment
Photothermal material
Salt-resistance
Durability

ABSTRACT

The utilization of solar-driven interfacial evaporation technology is highly important in addressing the energy crisis and water scarcity, primarily because of its affordability and minimal energy usage. Enhancing the performance of solar energy evaporation and minimizing material degradation during application can be achieved through the design of novel photothermal materials. In solar interfacial evaporation, photothermal materials exhibit a wide range of additional characteristics, but a systematic overview is lacking. This paper encompasses an examination of various categories and principles pertaining to photothermal materials, as well as the structural design considerations for salt-resistant materials. Additionally, we discuss the versatile uses of this appealing technology in different sectors related to energy and the environment. Furthermore, potential solutions to enhance the durability of photothermal materials are also highlighted, such as the rational design of micro/nano-structures, the use of adhesives, the addition of anti-corrosion coatings, and the preparation of self-healing surfaces. The objective of this review is to offer a viable resolution for the logical creation of high-performance photothermal substances, presenting a guide for the forthcoming advancement of solar evaporation technology.

1. Introduction

With population growth and urbanization, coupled with climate change and environmental pollution, water environmental problems are becoming increasingly prominent worldwide, including water shortage, water pollution and water resource degradation, especially in developing countries [1,2]. Around 2050, it is projected that approximately four billion individuals across the globe will experience water scarcity issues [3].

To address the issue of limited availability of fresh water resources, numerous methods for desalinating seawater have been extensively researched, including reverse osmosis, distillation, multi-stage flash evaporation, electrodialysis, and others [4–6]. However, these methods consume a significant amount of energy. Currently, global energy consumption is predominantly reliant on non-renewable fossil fuels, which not only deplete natural resources but also have substantial environmental implications. Hence, it is imperative to discover a technique for desalinating seawater that can utilize renewable energy sources. As a kind of abundant renewable clean energy and low cost, solar energy has attracted the attention of researchers. Simultaneously, to address the issue of heat loss resulting from the heating of the entire water body during solar energy evaporation, a solar-driven interfacial evaporation technology is proposed. This approach localizes photogenerated heat on material surfaces and efficiently facilitates seawater evaporation by selectively heating a small amount of water [7,8]. This technology is of great significance to alleviate the scarcity of water resources and promote the sustainable growth of energy. Therefore, the solar-driven interfacial evaporation technology has immense promise in the advancement and utilization of freshwater resources.

In the past few years, the research on solar-driven interfacial evaporation technology has mainly focused on the development of photothermal conversion materials with excellent performance. The ideal materials should include the following characteristics: (1) The material that can absorb sunlight across the full spectral range; (2) The materials possesses a favorable pore structure, facilitating rapid water transfer, and exhibits exceptional thermal insulation properties to prevent heat loss to the surrounding water; (3) The

* Corresponding authors.
E-mail addresses: hmgao0621@163.com (H. Gao), 200201030001@hhu.edu.cn (Z. Li), Xingtao.xu@zjou.edu.cn (X. Xu).

https://doi.org/10.1016/j.cclet.2024.109925
1001-8417/

materials are eco-friendly, affordable, stable and easy to large-scale production [9,10].

Nowadays, with the continuous development of material science, numerous excellent photothermal materials have been created, leading to a wider range of applications for these materials.

The main focus of this paper is to present a thorough review of the main categories and principles of action for photothermal materials, as well as the structural design of salt-resistant photothermal materials. Additionally, it introduces various applications of photothermal materials in fields beyond seawater desalination and discusses strategies for improving their durability.

2. Categorization of typical photothermal materials

The primary process involved in evaporation is the conversion of solar energy into heat energy. The efficiency of evaporation is directly influenced by the photothermal materials on the device's surface. When selecting materials, it is crucial to take into account their sunlight absorption rate and their efficiency in converting it. It is advisable to choose photothermal materials that have a high absorption rate, low transmission, and reflection ratio as much as possible [11]. Therefore, the advancement of materials is vital for driving the technology of solar-driven interfacial evaporation. At present, the primary materials utilized encompass metal materials, semiconductor materials, carbon-based materials, and polymer materials [11,12]. The examples of typical photothermal materials are introduced in Supporting information.

2.1. Metal materials

Metal nanomaterials exhibit a high capacity for sunlight absorption and thermal conversion, primarily achieved through the phenomenon of localized surface plasmon resonance [13]. When the incident light's frequency aligns with the vibration frequency of the nanoparticles' electrons, the electrons become excited and generate hot electrons, then the hot electrons resonate with the electromagnetic field of the incident light, leading to the conversion of light energy into heat energy [14]. Metal nanoparticles such as gold (Au), silver (Ag), copper (Cu), and aluminum (Al), are widely utilized materials in various applications.

2.2. Semiconductor materials

Semiconductor materials, being a novel form of photothermal conversion material, have extensive applications in the field of photothermal technology due to their diverse range, convenient functionalization, and affordable price [15]. According to the photothermal conversion principle, semiconductor materials can be classified into two categories. The first material under consideration is a semiconductor with a defect structure, which cause the migration of carriers on the material's surface, resulting in a local plasmon resonance effect that is similar to the surface of metal nanoparticles, and photothermal conversion occurs, such as some copper chalcogenides [16]. The second is a semiconductor material with an intrinsic absorption band gap. When semiconductor materials are exposed to light, the electrons present in the valence band absorb energy and shift to the conduction band, resulting in the creation of electron-hole pairs above the band gap, and then the electrons and holes relax to the edge of the energy band, and the energy beyond the band gap is converted into heat through a thermal relaxation process, such as transition metals and their nitrides, carbides, borides, and sulfides [17,18].

2.3. Carbon-based materials

In comparison to metal and semiconductor materials, carbon-based materials offer several advantages. Firstly, they are more cost-effective and abundant. Additionally, carbon-based materials exhibit excellent resistance to salt, acid, and alkali, making them highly versatile. Examples of such materials include carbon black, carbon nanotubes, and graphene. Moreover, carbon-based materials are known for their environmentally friendly properties. The material exhibits exceptional light absorption capabilities and demonstrates high photothermal conversion efficiency across the entire spectral range, making it extensively employed in the realm of seawater desalination [19]. When sunlight irradiates carbon-based materials, the electrons absorb energy and transition from the ground state to the excited state. Upon the return of electrons from an excited state to the ground state, the previously absorbed light energy can be converted into heat energy through the vibration of the lattice and subsequently released [20].

2.4. Polymer-based materials

Polymer materials possess several notable characteristics, including ease of synthesis, affordability, high light absorption rate, and good biocompatibility. In the past few years, solar-driven interfacial evaporation technology has witnessed widespread utilization of these materials. When subjected to illumination, the material undergoes a process where absorbed photons induce a rapid transition of electrons from the ground state to the excited state, and then the electrons in the excited state release heat energy (*i.e.*, photothermal effect) through non-radiative decay [21]. Common examples of organic polymer materials include polypyrrole (PPy) and polydopamine (PDA).

Based on a brief overview and examples of the photothermal conversion principles of the above four types of photothermal materials, Table S1 (Supporting information) has been created. The simulated light intensity in the laboratory is 1 kW/m^2. The solar interfacial evaporation devices, fabricated using carbon-based materials and polymer materials, exhibit a comparatively high evaporation rate and are cost-effective. Consequently, these devices hold significant potential for widespread utilization in the future.

3. Salt-resistant design of photothermal materials

When the evaporation device is operating in brine environment, water and solute are transported through non-selective capillaries, and salt ions will diffuse back to the bulk liquid due to the concentration gradient, but some of them will remain in the porous channel and begin to crystallize when saturated [22]. Simultaneously, the deposition of salt on the surface of the photothermal material can obstruct sunlight, resulting in a substantial evaporation effectiveness reduction. At present, the elimination of salt crystals necessitates cleaning or post-treatment methods to restore the functionality of the evaporator. This subsequently results in a rise in production expenses. In order to tackle the problem of salt accumulation during interfacial evaporation, it is imperative to explore novel photothermal materials that exhibit resistance to salt. Currently, there are several methods to enhance the salt resistance of evaporation devices. These include increasing the flow of water to remove salt, manufacturing Janus double-layer structure or superhydrophobic coating to limit salt intrusion and using ion repulsion effect [23,24]. The examples of salt-resistant design are shown in Figs. S5-S7 (Supporting information).

3.1. Structural design to enhance water flow

As is widely recognized, solar interfacial evaporation devices function exclusively during daylight hours, with their evaporation efficiency steadily increasing until noon. With the process of evaporation, the concentration of salt in the device gradually increases,

resulting in the formation of a concentration difference. As the process of salt crystallization occurs, the ongoing influx of water will dissolve the salt and cause it to revert back into the seawater [25,26]. This phenomenon demonstrates inherent self-cleaning characteristics, which can be further optimized to attain the salt-tolerant functionality of the device. The better the hydrophilicity and porosity of the material, the stronger the self-cleaning ability [27].

Carbonization of natural plant materials is an economically viable and well-established technique that has been effectively utilized in the fabrication of solar evaporators, resulting in exceptional performance. Wang *et al*. successfully synthesized a superhydrophilic porous carbon foam material through the process of slicing potatoes and subsequently subjecting them to carbonization at a temperature of 600 °C for 2 h [28]. The material exhibits a significantly porous structure with interconnected pores, as depicted in Fig. S5a (Supporting information). This unique structure facilitates efficient water transport and enables rapid dissolution of salt crystals within the three-dimensional porous framework. In the simulated seawater, there was no discernible salt accumulation was observed on the surface of the material after 8 h of 1 kW/m^2 light irradiation. Kuang *et al*. drilled holes along the growth direction of the wood block, and then carbonized the surface to form millimeter-scale (drilling) and micron-scale channels (Fig. S5b in Supporting information), which are low-salt concentration and high-salt concentration channels, respectively, and will form a concentration gradient, thereby achieving spontaneous salt exchange, so that the salt solution in the micron-scale channel is diluted, effectively preventing the accumulation of salt crystallization [29]. Chen *et al*. successfully fabricated a porous framework photothermal microgroove-structured aerogel (PDA/PEI/PPy@PI-MS MGA, pppMGA) by freeze-drying, laser engraving, and chemical polymerization techniques [30]. The resulting aerogel exhibited a three-dimensional skeleton, microgroove structure flume, and cotton core multistage efficient water delivery network (Fig. S5c in Supporting information). As the evaporation process advances, the presence of superhydrophilic microgrooves on the device's surface facilitates the ion exchange via capillary action, thereby decelerating the rate of salt crystallization. The low-concentration brine present in the microgrooves simultaneously dissolves the crystals and inhibits their further accumulation, thereby demonstrating a consistent and effective evaporation capability.

This kind of photothermal material has excellent ability to transport water, which can accelerate the diffusion of salt ions, dilute the salt concentration at the evaporation interface, avoid the formation of salt crystals, and effectively enhance the salt resistance of the evaporation device. Nevertheless, a portion of the thermal energy is frequently dissipated during the process of diffusion, thereby exerting an influence on the rate of evaporation to some degree.

3.2. Superhydrophobic coating and Janus structure

The presence of a superhydrophobic layer hinders the further transport of water towards the photothermal layer, and the salt that accumulates beneath the superhydrophobic layer will dissolve as the pumping process continues, ultimately returning to the salt water, which overcomes the limitations associated with fully hydrophilic structure being susceptible to erosion by seawater, as well as the slow evaporation rate of fully hydrophobic structures [31]. The design of the super-hydrophobic layer incorporates two distinct types of independent superhydrophobic coating and a Janus structure [32].

For the purpose of developing superhydrophobic coatings, Shen *et al*. prepared a flexible superhydrophobic photothermal membrane (CNTs@PVP) with a water contact angle of 150.8°, which is composed of polyvinyl pyrrolidone (PVP) and carbon nanotubes (CNTs) with 1*H*,1*H*,2*H*,2*H*-perfluorodecyl triethoxysilane modification (Fig. S6a in Supporting information) [33]. The excellent hydrophobicity of the material contributes to its outstanding resistance to salt. Following 40 h of uninterrupted operation and 18 cycles of evaporation, there was no build-up of salt and no significant decline in the rate of evaporation.

The Janus membrane is characterized by its asymmetry, featuring superhydrophobicity on one side and superhydrophilicity on the other side. The utilization of a super-hydrophobic layer is employed for the purpose of photothermal conversion, whereas the super-hydrophilic layer serves as a means of water transportation. Due to the hindrance of the superhydrophobic layer, water stops when it reaches the hydrophilic/hydrophobic interface, and the evaporation process occurs at this interface to prevent salt intrusion [34]. Song *et al*. prepared a Janus solar evaporation device based on PPy-coated porous structure nickel sponge (NSP) (Fig. S6b in Supporting information) [35]. The absence of hydrophilic functional groups is responsible for the weak interaction between the PPy film and water molecules. Moreover, the coarse texture of the sample and the abundance of air cushions inside it enhance its superhydrophobic properties. This is demonstrated by a water contact angle measuring 150.3°. Following the modification of sodium alginate, the lower part of the specimen exhibits superhydrophilicity, which is supported by a contact angle measurement of 0°. The evaporator's asymmetrical wettability effectively hinders salt deposition, demonstrating exceptional resistance to salt even when exposed to simulated salt water with a concentration of 15%. Hu *et al*. designed a Janus carbon nanotube@Poly(butylene adipate-*co*-terephthalate) (PBAT) fabric (JCPF) and prepared a three-dimensional water channel evaporator (3D WCE), as shown in Fig. S6c (Supporting information) [36]. By adding appropriate content of carbon nanotubes, multi-level micro/nanostructures with porous microstructure and hairy nanostructures were obtained. These unique structures improve the surface hydrophobicity (water contact angle is 160°). When tested in simulated seawater, the fabric demonstrates remarkable light absorption and photothermal conversion properties, leading to an evaporation rate of 1.576 kg m^{-2} h^{-1} and an impressive energy conversion efficiency of 92.7%. In addition, it was observed that no salt particles were generated even after 8 h of uninterrupted operation in a 20% high concentration brine, showing long-term operational stability. It is worth noting that the photothermal film is environmentally friendly and can be naturally degraded after the end of service life.

The superhydrophobicity design can effectively prevent salt accumulation. However, the existing methods of modification result in significant costs and hinder production expansion. In the future, it is imperative to further decrease the expenses associated with modification.

3.3. ion repulsion effect

By implementing an ion barrier, the Donnan effect is used to repel the accumulation of salt by repelling ions of the same charge in the salt solution [23]. For instance, Wang *et al*. first reported the self-desalination photothermal material of monolithic porous ionic polymers (PIPs) coated with PPy [23]. The polymer that incorporates the imidazolium cation group exhibits a repulsive effect on the cations present in the solution (Fig. S7a in Supporting information). This characteristic enables the polymer to demonstrate a highly effective and stable evaporation capacity when exposed to simulated seawater containing 30% NaCl concentration.

Similarly, Xiao *et al*. developed Janus photothermal materials by utilizing a porous superhydrophilic poly(ionic liquid) monolith

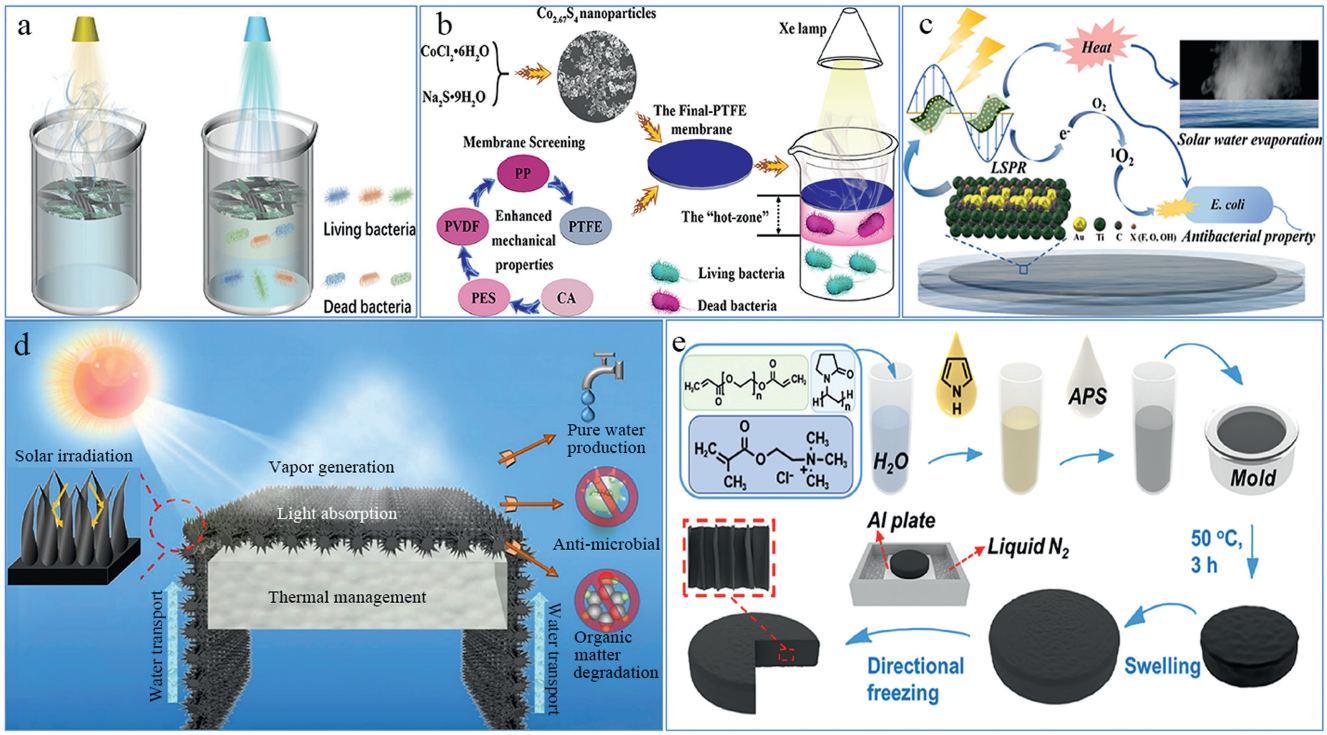

Fig. 1. Antibacterial effect: (a) Schematic illustrations of the photothermal water evaporation and photothermal bacterial killing, based on borophene-embedded cellulose papers. Copied with permission [40]. Copyright 2023, Wiley. (b) Schematic illustration of the synthetic method, efficient solar water evaporation, and thermal antibacterial property. Copied with permission [41]. Copyright 2019, American Chemical Society. (c) Schematic illustration of the Au/Ti_3C_2 photothermal membrane with antibacterial ability. Copied with permission [43]. Copyright 2021, American Chemical Society. (d) Schematic illustration CuO nanowire tree system. Reproduced with permission [44]. Copyright 2019, American Chemical Society. (e) Schematic illustration of the preparation of CPHs. Copied with permission [45]. Copyright 2021, American Chemical Society.

that was coated with hydrophobic carbon soot (C-PDVB-BFILs) to achieve efficient solar steam generation [37]. The repulsive effect of poly(ionic liquid) imidazolium cations on cations in a salt solution was synergistically combined with a Janus structure, resulting in remarkable salt resistance, as depicted in Fig. S7b (Supporting information). No salt crystals were observed to precipitate during a continuous 6 h operation in a 20% saline solution. Li *et al.* constructed a cost-effective Janus complex (JC) by combining commercial carbon nanotubes and porous cotton fiber paper (PCFP) through the process of silanization and the combination of polyelectrolyte (PDDA) [38]. The resulting complex was named t-OCNTs/PCFP JC (Fig. S7c in Supporting information). The strong ionic strength of PDDA renders it effective in preventing salt deposition during solar seawater desalination, thereby highlighting its potential for application in this field.

Compared to the aforementioned materials, it is evident that the design of salt-resistant photothermal materials is not constrained by a single principle. In order to produce materials with exceptional performance, it is often necessary to employ a combination of various technologies in a synergistic manner to enhance the overall effect.

The evaluation of salt resistance performance is based on the presence of salt crystallization on the surface of the evaporation device and the evaporation rate during testing. Subsequently, the following Table S2 (Supporting information) is compiled to categorize different photothermal materials based on their salt resistance properties. In relation to the present circumstances, various designs have demonstrated significant salt tolerance. Even under extreme conditions, such as exposure to a 20% NaCl solution or a 30% NaCl solution, these designs are able to maintain a certain level of salt tolerance. This capability greatly enhances the longevity of the evaporation device.

4. Development of other functions of photothermal materials

With the advancement of scientific and technological research, a plethora of photothermal materials have been successfully developed. Consequently, the efficiency of solar energy utilization has witnessed a steady improvement, thereby facilitating the progress of solar-driven interfacial evaporation technology. However, the practical implementation of single-function solar evaporation devices is constrained, thus necessitating the development of multifunctional evaporation devices based on photothermal materials. For example, photothermal membranes with antibacterial effect, photothermal catalysis, pollutant degradation adsorption.

4.1. Antibacterial effect

In the practical application of solar interfacial evaporation, the presence of microbial accumulation on the device's surface poses challenges. This leads to pollution of the photothermal membranes, blockage of the water transmission channel, and subsequent negative impacts on the photothermal conversion capacity, evaporation efficiency, and overall device lifespan [39]. To tackle the previously mentioned problems, it is crucial to create a photothermal film that possesses antibacterial properties.

Given that the photothermal material can produce high temperatures during operation, it can effectively eliminate bacteria due to the thermal effect. Therefore, the inherent thermal properties of the device can be harnessed for this purpose. Guan *et al.* incorporated 2D borophene nanosheets into cellulose nanofibers (CNF) paper, resulting in the fabrication of flexible borophene papers (Fig. 1a) [40]. Under 3 kW/m^2 illumination, almost 100% of Gram-positive and Gram-negative bacteria were killed within 20 min. Zhao *et al.* prepared $Co_{2.67}S_4$ nanoparticles deposited polytetraflu-

oroethylene (PTFE) membrane, which has demonstrated significant antibacterial properties, effectively inhibiting bacterial growth, as depicted in Fig. 1b [41]. However, the antibacterial efficacy of these devices is solely reliant on the photothermal effect, making it highly susceptible to variations in light conditions. Consequently, its practical application yields suboptimal results.

Metal materials (such as Au, Ag) can generally achieve broadband absorption after adjusting the shape, and have good antibacterial activity [42]. For example, Qu's team reported a multifunctional Au/Ti_3C_2 photothermal membrane (Fig. 1c) with stable antibacterial ability, which has physical and chemical antibacterial effects: Through the excellent photothermal properties of the material, high temperature is generated, resulting in the destruction of the cell wall of the bacteria under the thermal process, and then death; in addition, AuNPs and Ti_3C_2 in the membrane can produce reactive oxygen species (singlet oxygen), which can effectively inactivate bacteria [43]. The photothermal membrane inactivated 6.7 $\log_{10}$ CFU/mL *E. coli* K-12 and 7.1 $\log_{10}$ CFU/mL *Spinopyxis* sp. BM1–1 within 20 min and 10 min, respectively. Although the sterilization of the material is highly effective, the doping of gold nanoparticles means high production costs. Therefore, it is recommended to explore alternative materials that are more cost-effective for future applications. Xu *et al*. developed a multifunctional photothermal material based on copper mesh with abundant CuO nanowires, as depicted in Fig. 1d [44]. The continuous release of copper ions has been found to effectively inhibit bacterial growth and demonstrate positive results in treating domestic sewage. The practical applications of photothermal materials have demonstrated significant antibacterial properties due to their inherent thermal effects and the unique characteristics of metal materials. These combined factors have led to promising results in the field. Peng *et al*. developed a cationic photothermal hydrogel (CPHs) using methacryloyloxyethyl trimethyl ammonium chloride (METAC) and polypyrrole (PPy) as raw materials (Fig. 1e) [45]. Because CPHs contain a large number of ammonium groups within the network, they can effectively kill *E. coli* and *Staphylococcus aureus*.

4.2. Pollutant treatment

Due to population growth and industrial development, a large number of pollutants have been discharged into the marine water body, which makes the marine environment deteriorating and threatens the survival of human beings [46]. Therefore, our objective is to develop multifunctional photothermal materials capable of efficiently treating pollutants, as well as purifying water through desalination.

It is well known that when some pollutants such as phenol, aldehyde and ketone enter seawater, they will form azeotrope solution, which will be degraded into carbon dioxide and water during evaporation [47]. Based on this principle, Noureen *et al*. developed multifunctional Ag_3PO_4-reduced graphene oxide (Ag_3PO_4-rGO) nanocomposite-coated textiles, which can completely decompose rhodamine B (RhB) in the experiment, as shown in Fig. S8a (Supporting information) [48]. Furthermore, the photocatalytic properties of the material remain unaltered even after undergoing five cycles. Zhang *et al*. prepared reduced graphene oxide/carbon nitride composite sponge (rGO-g-C_3N_4-PVA-PU) (Fig. S8b in Supporting information) for solar evaporation and wastewater treatment [49]. The degradation rates of methylene blue and RhB were found to be remarkably high, reaching 99.20% and 91.07% respectively. Tu *et al*. sucessfully synthesized a multifunctional mesoporous Ag@MnOx/m-SiO_2 (AMSs) nanocomposite, as shown in Fig. 2a [50]. This material not only has excellent photothermal properties (1.51 kg m^{-2} h^{-1}) and antibacterial ability, but also can degrade nitrophenol. Du *et al*. constructed a dual-functional photothermal nanosphere by integrating ultrafine plasma Co_3O_4 into a nitrogen-doped carbon layer over silica nanospheres (SiO_2@Co/C), as dipicted in Fig. 2b [51]. This material can effectively treat bisphenol A. It also has good degradation effects on oxytetracycline and tetracycline, shows its potential in the treatment of environmental antibiotic pollution. Li's group have used Prussian blue analogue (PBAs) as precursors to prepare $FeNi_3$/graphitic carbon nanofibers-3 (CNT-3) through electrospinning and carbonization methods, as shown in Fig. S8c (Supporting information) [52]. The synergistic effect of $FeNi_3$ and graphitized CNF can promote the photothermal efficiency and effectively degrade organic dyes. Du *et al*. used self-assembly methods and tuning calcination to prepare SiO_2@CoFe/C nanosphere materials (Fig. S9a in Supporting information) [53]. The introduction of Co can effectively improve the activity of peroxymonosulfate, resulting in a certain degree of catalytic degradation synergy. This study provides significant enlightenment for the comprehensive application of photothermal materials in pollutant separation and fresh water regeneration.

On the other hand, physical adsorption offers the benefits of affordability and high efficiency, but the accumulation of pollutants on solar energy absorption materials will cause the absorption rate of light to decrease, so it is more practical for sewage treatment with low pollution [17]. Wang *et al*. reported on the development of a carbonized cattail-agarose hydrogel (CCAH) membrane with many microchannels resembling bamboo knots, which has excellent hydrophilicity, light absorption capacity and pollutant adsorption capacity (Fig. 2c) [54]. Its evaporation rate and evaporation efficiency reached 1.93 kg m^{-2} h^{-1} and 95.8% under 1 sun irradiation. In experiments involving the treatment of heavy metal wastewater (Cr^{2+}, Cd^{+}, and Pb^{2+}) at both low concentration (10 mg/L) and high concentration (100 mg/L), the rejection rate exceeded 99.9%. Similarly, in simulated dye wastewater experiments using RhB, methyl orange, and methyl blue at a concentration of 10 mg/L, the rejection rate reached an impressive 99.7%. The CCAH membrane exhibits exceptional water treatment capabilities, making it highly promising for applications in seawater desalination and sewage treatment.

Nowadays, there is a frequent occurrence of marine oil spill accidents, which significantly and adversely affect the environment [55]. In order to address this issue, people have invested a lot of resources to develop adsorption materials for removing oil pollution, but these materials are very ineffective in removing heavy oil, because heavy oil has a great viscosity at room temperature (10^3-10^5 mPa·s), which poses a significant challenge in terms of penetrating the pores of the adsorbent [56]. Nevertheless, as the temperature rises, the viscosity of heavy oil will progressively decrease [57]. Therefore, the photothermal effect can be utilized to decrease viscosity and facilitate the development of photothermal adsorption materials capable of in situ adsorption of heavy oil. Chang *et al*. prepared a photothermal adsorbent with superhydrophobicity and superoleophilicity by using carbon nanotube (CNT) modified polyurethane sponge (Fig. S9b in Supporting information) [58]. The adsorbent can effectively heat the heavy oil at the oil-sponge interface, reducing its viscosity by two orders of magnitude. This allows the modified sponge to absorb 20 times its own weight of heavy oil quickly when exposed to sunlight irradiation. When the adsorbent undergoes the process of oil adsorption, it is imperative to take into account both the oil recovery and the absorbent regeneration. Wu *et al*. incorporated PPy with photothermal conversion capabilities and poly(N-isopropylacrylamide) (PNIPAm) with thermal response properties into a melamine sponge, resulting in the synthesis of PNIPAM/PPy functionalized sponges [59]. Due to its hydrophobic nature above 32 °C and hydrophilic nature below 32 °C, PNIPAm/PPy exhibits the ability to passively release heavy oil at room temperature following heavy oil treatment, as shown in Fig. 2d. This release process does not necessitate the use of ex-

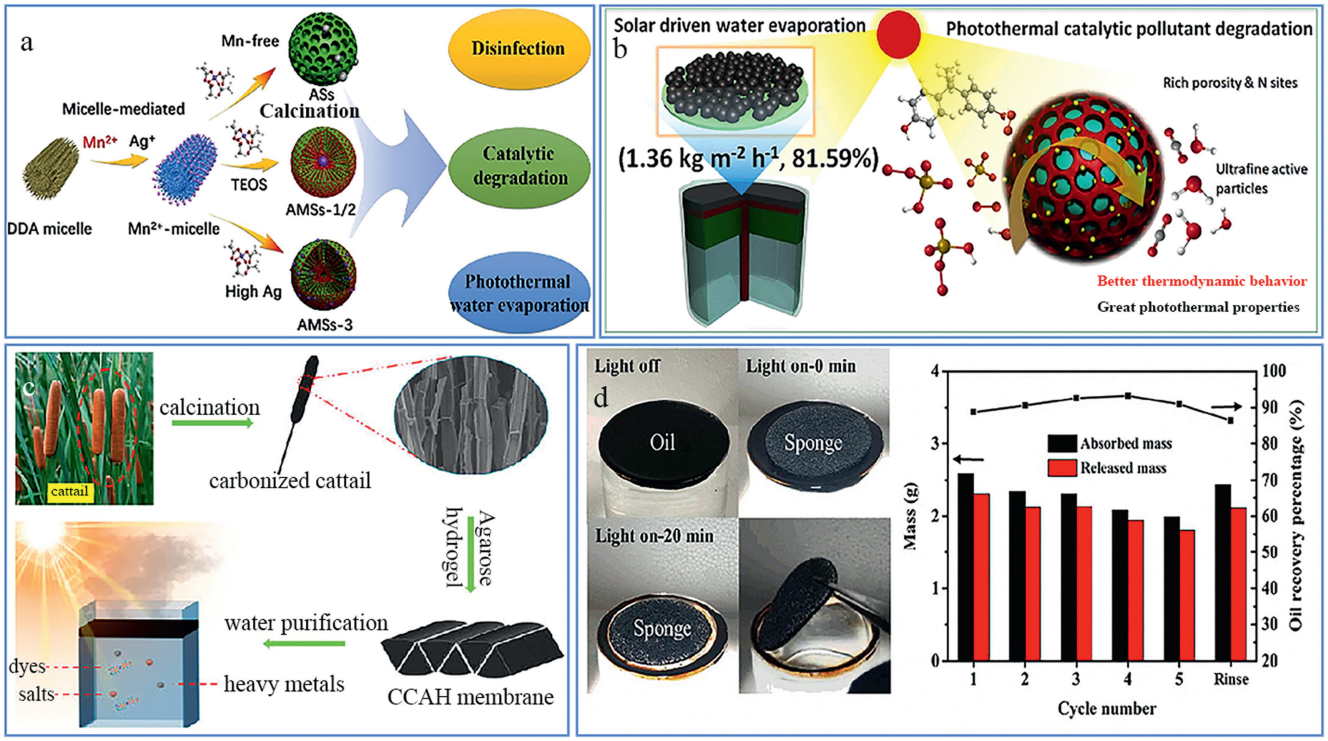

Fig. 2. Pollutant treatment. (a) Schematic of multifunctional Micelle-mediated metal assembly strategy for the synthesis of the Ag@MnOx/m-SiO_2 nanosphere. Copied with permission [50]. Copyright 2022, Elsevier. (b) The SiO_2@Co/C photothermal nanosphere with optimal abundant active sites. Copied with permission [51]. Copyright 2023, Elsevier. (c) Schematic diagram of preparation process and application of carbonized cattail–agarose hydrogel (CCAH) composite membrane for solar water evaporation and water purification. Copied with permission [54]. Copyright 2021, American Chemical Society. (d) Schematic illustration of the fabrication process of PNIPAm/PPy@MS and absorption of mineral oil experiment. Copied with permission [59]. Copyright 2018, Wiley.

tra energy, conserves resources, and holds greater significance for sustainable development.

Currently, solar interfacial evaporation technology predominantly relies on photodegradation and physical adsorption for the purpose of sewage purification, and has demonstrated significant progress. It is important to acknowledge that when the device is in operation, the high temperature it generates can cause certain volatile organic pollutants in the water to evaporate, leading to their presence in the collected fresh water. Therefore, it is necessary to undertake further research and development of novel photothermal materials to effectively address the issue of pollutants in the future.

5. Durability of the photothermal materials

Conventional photothermal materials are susceptible to developing cracks or fractures when exposed to repetitive loads because of their inherent lack of flexibility or fragility in structure [60,61]. Furthermore, it typically leads to a decrease in energy harvesting efficiency in real-word applications. Therefor the chemical stability and mechanical strength of the photothermal materials need further attention for future applications and the more complex situation faced by the evaporation device in practical application [62]. At present, there are some strategies to improve the durability such as the rational design of micro/nano-structures, the use of adhesives, the addition of anti-corrosion coatings, and the preparation of self-healing surfaces [63].

Huang *et al.* suggested a highly durable photothermal material by combining liquid metals (LMs) with polymers through dynamic crosslinking, leveraging the distinctive mechanical deformability of LMs [64]. During the stretching process, the polymer chains can undergo orientational crystallization, while the embedded core-shell structured LMs droplets are squeezed using the dynamically cross-linked interface, as shown in Fig. 3a. The resulting composite has a highly aligned structure, thus demonstrating exceptional mechanical properties. Its tensile strength measures 283.7 MPa, enabling it to support a weight 200,000 times its own. The LMs dispersed in the polymer skeleton makes the material flexible and long-term structural reliability, the material can bear 100,000 cycles. Ren *et al.* designed a highly efficient solar steam making device, Cu nanoparticles encapsulated in ultra-thin graphene were *in-situ* grown on carbonized loofah sponge by pyrolysis of metal-organic skeleton and natural loofah sponge biomass (Fig. 3b) [65]. The graphene sheets efficiently shield Cu from oxidation in normal surroundings, which is advantageous for achieving the plasmonic heating of Cu^0 during solar vapor generation. Xie *et al.* designed and fabricated a micro/nanostructured polyethylene/carbon nanotubes foam with interconnected open-cell structure and graphite oxide/carbon nanotubes (GO@CNTs) coating (MN-PCG) using micro extrusion compression molding (μ-ECM) method [66]. Due to the strong bonding between the polyethylene framework and the F-GO@CNTs resulting from μ-ECM, the surface of the MN-PCG foam displays a uniform arrangement of primary micropillars, as shown in Fig. S10 (Supporting information).

These micropillars are then adorned with secondary microstructures in a consistent pattern. Due to the micro/nanostructures on its surface, the MN-PCG foam demonstrates excellent superhydrophobicity and possesses adequate resistance to acid/alkali. These surface features ensure the adaptability and durability of the foam. Wang *et al.* fabricated an inverted pyramid microstructure by embossing technology, and filled the interior of the structure with silica nanoparticles, so that the structure has excellent wear resistance and can still maintain strong hydrophobicity after one thousand friction experiments, as depicted in Fig. S11 (Supporting information) [67]. The rational design of micro/nano-structures is excellent, but it requires subtle and

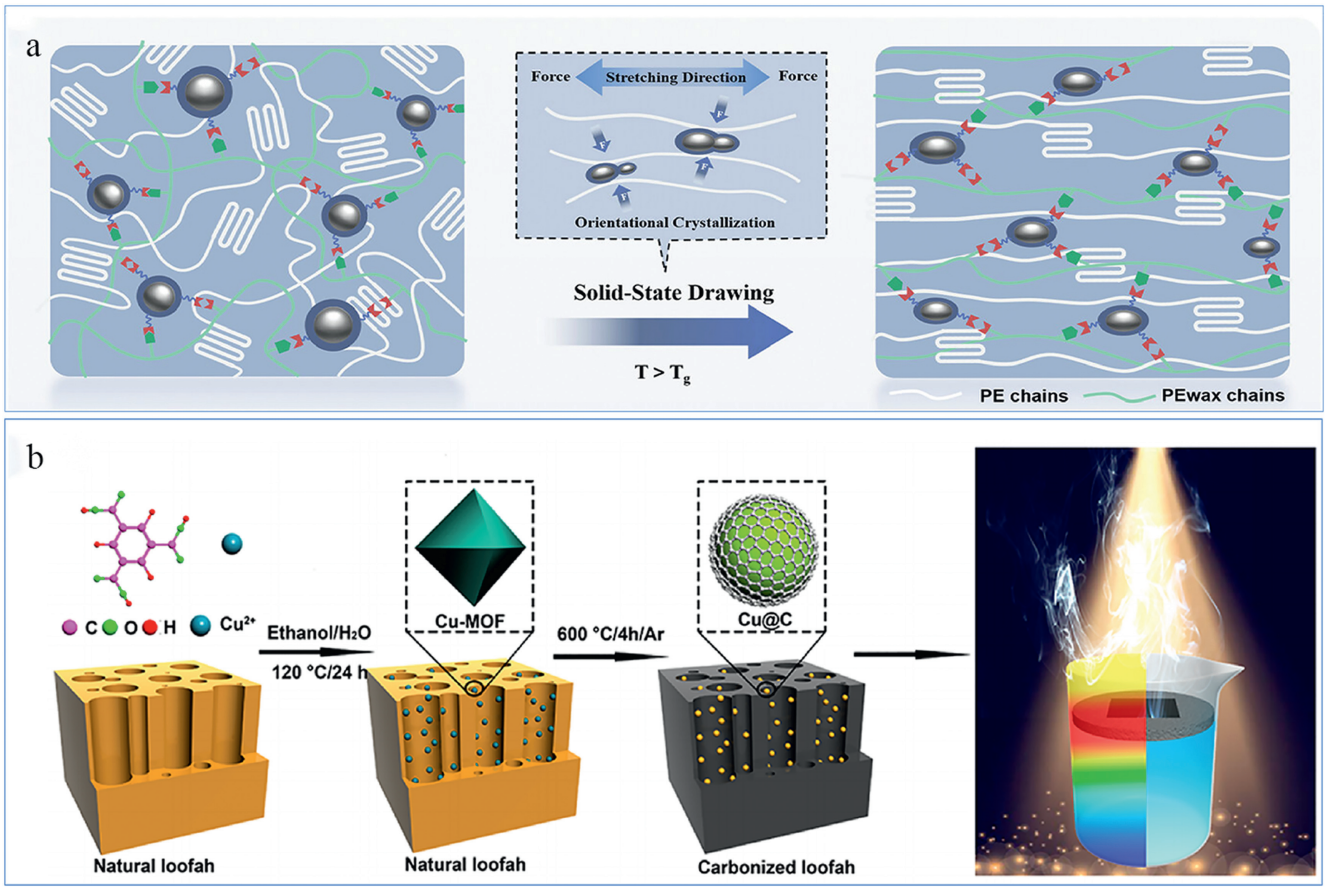

Fig. 3. Rational design of micro/nano-structures: (a) Schematic illustration of the bionic hierarchical architecture modulation, functionalized core–shell structure of LMs, efficient photothermal conversion and mechanical durable structure. Reproduced with permission [64]. Copyright 2022, Wiley. (b) Schematic illustration for the synthesis of a Cu@C/CLS structure. Copied with permission [65]. Copyright 2021, American Chemical Society.

complex processing methods, so it is more difficult and expensive, but it has a good application prospect in some highly demanding environments.

The method of using adhesive is relatively simple, and the adhesives can be applied to materials that require fast speed, low cost, and good wear resistance [63]. Zhou *et al.* synthesized anisotropic silica with different morphologies by adding different silane coupling agents in an emulsion-based one-pot method, and then adhered the nanostructured film to the substrate using a commercial acrylic adhesive [68].

Gomez-Vidal applied different types of nickel-based MCrAlX coatings to the surface of stainless steel, and the best coating can control the corrosion rate of stainless steel at 190 μm/year, which is 96% lower than that without the coating. This special coating is pre-oxidized within 24 h, during which time a uniform and dense layer of alumina forms on the stainless-steel surface, which can be used to further protect the solar power application materials from corrosion (Figs. 4a-c) [69]. Kong *et al.* invented an innovative method for producing a flexible coating with superhydrophobic properties for thermal energy storage and photothermal conversion by applying a combination of mesoporous C@SiO_2 nanotubes, polydimethylsiloxane, and industrial paraffin wax onto cloth through spraying (Figs. 4d and e) [70]. The resulting film possesses excellent flexibility, allowing it to withstand various distortions, such as bending and twisting, and return to its original shape under normal atmospheric conditions.

The exceptional effectiveness of superhydrophobic coatings in preventing metal corrosion has garnered significant interest. However, the practical use of these applications is still hindered by inadequate longevity and stability, as well as the intricate process of preparation. Then numerous researchers have investigated self-healing superhydrophobic surfaces. In addition, researchers have proposed strategies for adding self-healing polymers to superhydrophobic materials [71]. Under specific circumstances, materials with self-repairing capabilities can help restore damaged regions on super water-repellent surfaces [72]. Wu *et al.* prepared a conductive superhydrophobic film by depositing a thermally healable polycaprolactone (PCL)/poly(vinyl alcohol) (PVA) composite film with silver nanoparticles (AgNPs) and silver nanowires (AgNPs-AgNWs), and then depositing 1*H*,1*H*,2*H*,2*H*-perfluorodecanethiol (Fig. 5a) [73]. The layer of AgNPs-AgNWs not only provides hierarchical structures at both micron-scale and nano-scales to enhance superhydrophobicity, but it also could be heated at low voltage or low power NIR light exposure to heal the PCL/PVA film underneath.

Han *et al.* created composites consisting of graphene/ZnO-dodecanethiol (G/ZnO-SH) in advance [74]. Next, the researchers mixed G/ZnO-SH composites with an organic resin and applied the mixture onto a metal substrate to obtain the EP-FEVE@G/ZnO-SH coating, as depicted in Fig. 5b. After undergoing O_2 plasma etching, the resulting coating can rapidly regain its superhydrophobic properties when exposed to 3.21 sun irradiation. The impaired layer can quickly warm up in the presence of sunlight, causing the hydrophobic alkyl chains located at the lower part to move upward. This layer greatly enhances the durability of the superhydrophobic exterior and has significant potential in protecting metal surfaces from corrosion, thereby extending their lifespan. Li *et al.* fabricated a super-hydrophobic composite coating which used epoxy modified silicone resin polymers as film-forming substance and

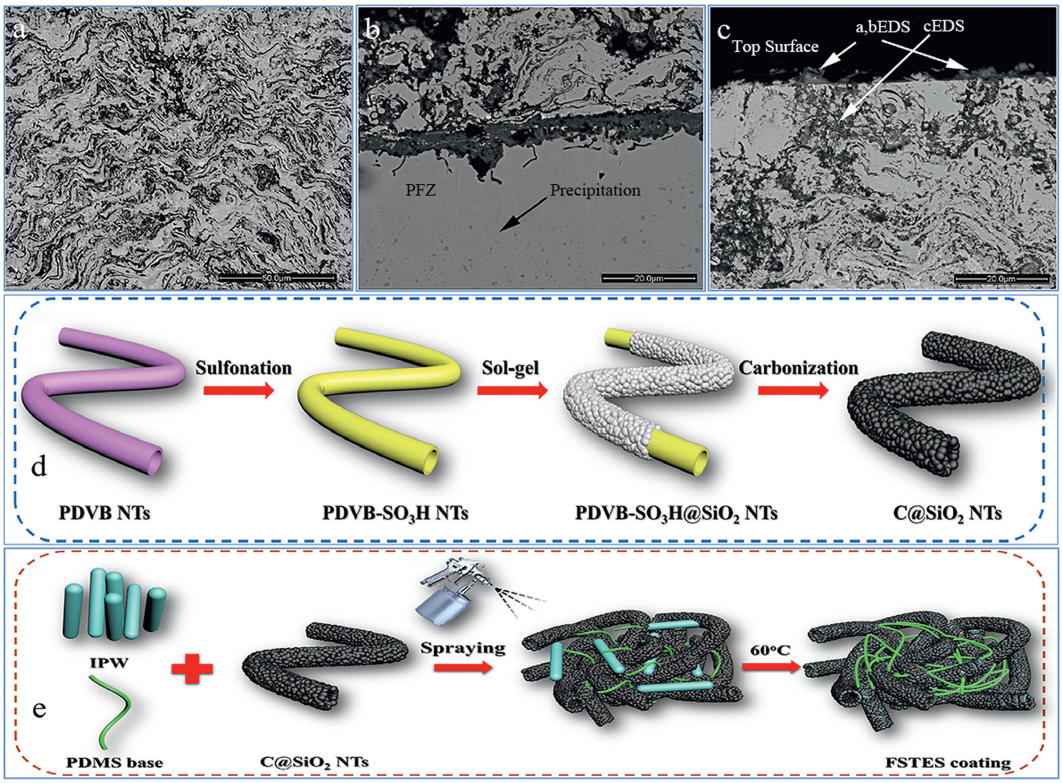

Fig. 4. The addition of anti-corrosion coatings: (a) BSE-SEM image of coating microstructure of oxidized HVOF–NiCoCrAlYTa away from the top surface and interface with steel; (b, c) BSE-SEM image of material exposed to NaCl–KCl at 700 °C showing microstructure at coating/steel interface and penetration at the outer surface of the top coating. Reproduced with permission [69]. Copyright 2017, Nature. (d) Preparation schematic illustration of $C@SiO_2$ NTs and (e) FSTES coating. Reproduced with permission [70]. Copyright 2022, Elsevier.

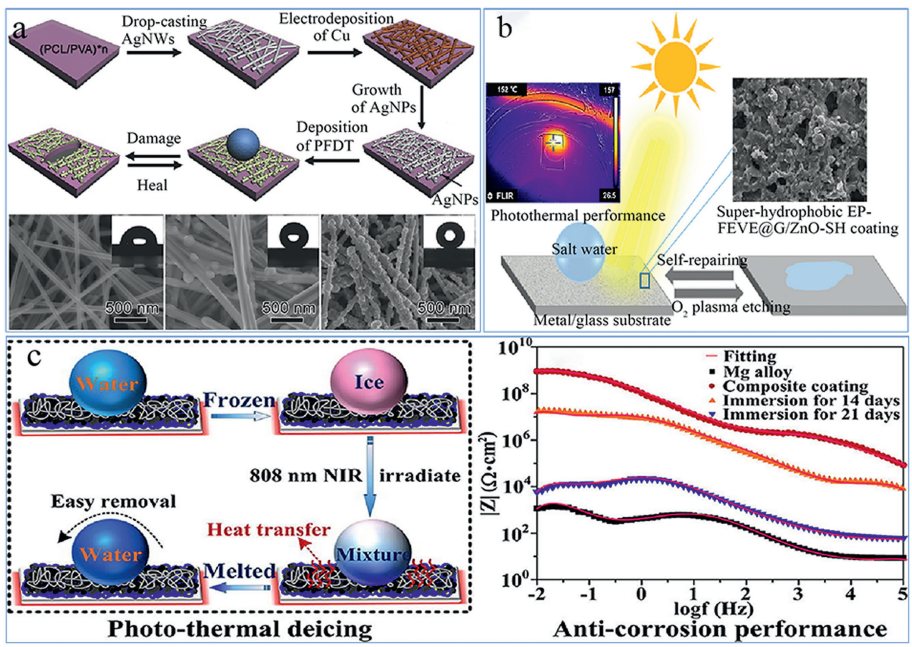

Fig. 5. The preparation of self-healing surfaces: (a) Schematic illustration of the fabrication process for healable superhydrophobic PFDT/AgNPs-AgNWs/(PCL/PVA) films and Top-view SEM images indicative of the AgNPs-AgNWs/(PCL/PVA) film fabrication process. Reproduced with permission [73]. Copyright 2016, American Chemical Society. (b) Schematic illustration of EP-FEVE@G/ZnO-SH. Reproduced with permission [74]. Copyright 2022, Elsevier. (c) Schematic illustration of robust and photo-thermal super-hydrophobic composite coating. Copied with permission [75]. Copyright 2022, Elsevier.

composite additive phases (modified SiO_2, Graphene oxide, TiC) was treated on several substrates [75]. The coating demonstrates outstanding mechanical, chemical, and durable properties, as well as long-lasting protection against corrosion with self-healing capabilities, as depicted in Fig. 5c.

Through one or more of the above strategies, it is expected to improve the durability of photothermal materials and further promote the progress of solar-driven evaporation interfacial technology.

6. Conclusions

Solar-driven interfacial evaporation technology has garnered significant attention as a clean, cost-effective, and efficient method for seawater desalination. After years of dedicated research and development, this technology has become increasingly mature. As the cornerstone of technological advancements, novel and highly efficient photothermal conversion materials have become the primary focus of ongoing research among scholars. Researchers aim to reduce costs and streamline processes while enhancing performance, thereby facilitating the practical implementation of this technology. Based on a comprehensive analysis of previous research findings, this paper provides a summary of the various categories of photothermal materials. It is evident that exceptional photothermal materials possess the attributes of a high absorption rate, favourable porosity, and thermal insulation performance. At the same time, they also strive to possess simple and easily attainable attributes in order to facilitate large-scale implementation.

Salt accumulation issues are frequently encountered during the routine operation of the interfacial evaporation device, thereby impeding the overall efficiency of evaporation. In this paper, an analysis is conducted to categorize the three existing types of salt-resistant photothermal materials that possess self-cleaning capabilities. Currently, a plethora of photothermal materials exhibiting exceptional resistance to salt have been developed, thereby ensuring prolonged and stable operation of evaporation devices. However, the current studies have only been conducted using simulated seawater or NaCl solutions, which provide a relatively simplistic environmental setting. If the findings are to be applied in practical settings, additional research is required.

In addition, this paper provides a concise overview of the various functionalities of photothermal materials, thereby demonstrating the potential application of solar-driven interfacial evaporation technology in intricate aquatic environments. Also, the application of solar-driven interfacial evaporation system needs to be further broadened, and the combination of seawater desalination with hydrogen production and power generation is also the main research direction in the future.

Finally, we analyzed the enhancements in the durability of photothermal materials and provided a brief summary of the existing methods. Each method exhibits distinct advantages and disadvantages. For instance, simple and low-cost adhesives offer general effectiveness, while self-healing surfaces and micro/nano-structures designs provide excellent performance but are complex to implement. Coatings, on the other hand, suffer from poor stability, and the manufacturing methods associated with them are challenging. Further development of robust long-term photothermal materials is still a bottleneck problem that needs to be solved. In order to achieve optimal results, it is imperative that we employ existing methodologies in a proficient manner and strive to comprehend the durability mechanisms of materials.

Generally, when designing photothermal materials for the future, one should consider not only the photothermal properties of the materials, but also their cost, environmental friendliness, stability, salt-resistance, and versatility. Simultaneously, the design and production of related efficient water collectors need urgent attention, as they are crucial for implementing solar-driven interface evaporation technology in practical applications.

Declaration of competing interest

The authors declare that they have no known competing financial interests or personal relationships that could have appeared to influence the work reported in this paper.

CRediT authorship contribution statement

Yiming Fang: Writing – original draft. **Huimin Gao:** Writing – review & editing. **Kaiting Cheng:** Data curation. **Liang Bai:** Data curation. **Zhengtong Li:** Conceptualization. **Yadong Zhao:** Writing – review & editing. **Xingtao Xu:** Writing – review & editing.

Acknowledgments

The work was financially supported by Zhejiang Provincial Natural Science Foundation of China (No. LR23C160001), and Scientific Research Startup Foundation of Zhejiang Ocean University (No. 11034150220006).

Supplementary materials

Supplementary material associated with this article can be found, in the online version, at doi:10.1016/j.cclet.2024.109925.

References

[1] J. Wu, X. Xuan, S. Zhang, et al., Chem. Eng. J. 473 (2023) 145421.
[2] H. Djuma, A. Bruggeman, M. Eliades, et al., Desalin. Water Treat. 57 (2016) 2290–2303.
[3] S. Zhang, X. Xu, X. Liu, et al., Mater. Horiz. 9 (2022) 1708–1716.
[4] X. Liu, X. Xu, X. Xuan, et al., J. Am. Chem. Soc. 145 (2023) 9242–9253.
[5] Z. Xing, X. Xuan, H. Hu, et al., Chem. Commun. 59 (2023) 4515–4518.
[6] X. Xu, M. Eguchi, Y. Asakura, et al., Energy Environ. Sci. 16 (2023) 1815–1820.
[7] D. Wei, C. Wang, J. Zhang, et al., Adv. Mater. 35 (2023) 2212100.
[8] T. Meng, Z. Li, Z. Wan, et al., Chem. Eng. J. 452 (2023) 139193.
[9] C. Song, M.S. Irshad, Z. Li, et al., Chem. Eng. J. 478 (2023) 146566.
[10] Y.C. Wang, L.B. Zhang, P. Wang, ACS Sustain Chem. Eng. 4 (2016) 1223–1230.
[11] F. Zhao, Y.H. Guo, X.Y. Zhou, et al., Nat. Rev. Mater. 5 (2020) 388–401.
[12] M.M. Gao, L.L. Zhu, C.K. Peh, et al., Energy Environ. Sci. 12 (2019) 841–864.
[13] Z.W. Seh, S.H. Liu, M. Low, et al., Adv. Mater. 24 (2012) 2310–2314.
[14] C.L. Wang, D. Astruc, Chem. Soc. Rev. 43 (2014) 7188–7216.
[15] I. Ibrahim, D.H. Seo, A.M. McDonagh, et al., Desalination 500 (2021) 114853.
[16] F.J. Tao, Y.L. Zhang, S.J. Cao, et al., Mater. Today Energy 9 (2018) 285–294.
[17] Y.X. Zhao, H.C. Pan, Y.B. Lou, et al., J. Am. Chem. Soc. 131 (2009) 4253–4261.
[18] C. Coughlan, M. Ibáñez, O. Dobrozhan, et al., Chem. Rev. 117 (2017) 5865–6109.
[19] W.X. Guan, Y.H. Guo, G.H. Yu, Small 17 (2021) 2007176.
[20] V.D. Dao, H.S. Choi, Glob. Chall. 2 (2018) 1700094.
[21] L.H. Xiao, X. Chen, X.Y. Yang, et al., ACS Appl. Polym. Mater. 2 (2020) 4273–4288.
[22] G.H. Liu, T. Chen, J.L. Xu, et al., Cell Rep. Phys. Sci. 2 (2021) 100310.
[23] F. Wang, Y.N. Su, Y.Z. Li, et al., ACS Appl. Energy Mater. 3 (2020) 8746–8754.
[24] Z.C. Wei, J. Wang, S. Guo, et al., Nano Res. 1 (2022) 9120014.
[25] M.W. Zhu, Y.J. Li, G. Chen, et al., Adv. Mater. 29 (2017) 1704107.
[26] Y.W. Yang, H.X. Feng, W.X. Que, et al., Adv. Funct. Mater. 33 (2023) 2210972.
[27] R.Q. Xu, H.Z. Cui, K.Y. Sun, et al., Chem. Eng. J. 446 (2022) 137275.
[28] C.B. Wang, J.L. Wang, Z.T. Li, et al., J. Mater. Chem. A 8 (2020) 9528–9535.
[29] Y.D. Kuang, C.J. Chen, S.M. He, et al., Adv. Mater. 31 (2019) 1900498.
[30] Z.C. Chen, Y.T. Luo, Q. Li, et al., ACS Appl. Mater. Interfaces 13 (2021) 40531–40542.
[31] J.Q. Zhao, Y.W. Yang, C.H. Yang, et al., J. Mater. Chem. A 6 (2018) 16196–16204.
[32] Y.W. Yang, H.Y. Zhao, Z.Y. Yin, et al., Mater. Horizons 5 (2018) 1143–1150.
[33] C. Shen, Y.Q. Zhu, X.D. Xiao, et al., ACS Appl. Mater. Interfaces 12 (2020) 35142–35151.
[34] F.Y. Wang, S.J. Zhao, X.Y. Zhang, et al., Desalination 543 (2022) 116085.
[35] R. Song, N.S. Zhang, P. Wang, et al., Appl. Surf. Sci. 616 (2023) 156448.
[36] N.N. Hu, S.L. Zhao, T.C. Chen, et al., ACS Appl. Mater. Interfaces 14 (2022) 46010–46022.
[37] C.H. Xiao, W.D. Liang, L.H. Chen, et al., ACS Appl. Energy Mater. 2 (2019) 8862–8870.
[38] D.D. Li, Q.X. Zhou, G. Wang, et al., J. Mater. Sci. 55 (2020) 15551–15561.
[39] W.Y. Duan, A. Dudchenko, E. Mende, et al., Environ. Sci. Process Impacts 16 (2014) 1300–1308.
[40] X.W. Guan, P. Kumar, Z.X. Li, et al., Adv. Sci. 10 (2023) 2205809.

[41] L. Zhao, Q.Z. Yang, W. Guo, et al., ACS Appl. Mater. Interfaces 11 (2019) 20820–20827.
[42] Y. Xu, J.X. Ma, Y. Han, et al., Chem. Eng. J. 384 (2020) 123379.
[43] W. Qu, H.N. Zhao, Q. Zhang, et al., ACS Sustain. Chem. Eng. 9 (2021) 11372–11387.
[44] Y. Xu, J.X. Ma, Y. Han, et al., ACS Sustain. Chem. Eng. 7 (2019) 5476–5485.
[45] B.L. Peng, Y.J. Gao, Q.Q. Lyu, et al., ACS Appl. Mater. Interfaces 13 (2021) 37724–37733.
[46] S.A. Kalogirou, Prog. Energy Combust. Sci. 31 (2005) 242–281.
[47] V.K.P. Janakey Devi, P.S.T. Sai, A.R. Balakrishnan, J. Chem. Eng. Data 63 (2018) 498–507.
[48] L. Noureen, Z.J. Xie, Y.J. Gao, et al., ACS Appl. Mater. Interfaces 12 (2020) 6343–6350.
[49] H. Zhang, L.L. Li, L. Geng, et al., Chemosphere 311 (2023) 137163.
[50] W. Tu, H. Li, B. Li, et al., J. Alloys Compd. 924 (2022) 166489.
[51] R. Du, H. Zhu, H. Zhao, et al., J. Alloys Compd. 940 (2023) 168816.
[52] H. Li, M. Aizudin, S. Yang, et al., Sep. Purif. Technol. 326 (2023) 124802.
[53] R. Du, H. Zhu, H. Zhao, et al., Environ. Res. 222 (2023) 115365.
[54] L. Wang, J.L. Wei, C. Zhou, et al., Membranes-Basel 12 (2022) 1076.
[55] D. Fragouli, A. Athanassiou, Nat. Nanotechnol. 12 (2017) 406–407.
[56] J. Ge, L.A. Shi, Y.C. Wang, et al., Nat. Nanotechnol. 12 (2017) 434–440.
[57] O. Alomair, M. Jumaa, A. Alkoriem, et al., J. Pet. Explor. Prod. Technol. 6 (2016) 253–263.
[58] J. Chang, Y.S. Shi, M.C. Wu, et al., J. Mater. Chem. A 6 (2018) 9192–9199.
[59] M.C. Wu, Y.S. Shi, J. Chang, et al., Adv. Mater. Interfaces 5 (2018) 1800412.
[60] Y.H. Guo, X.Y. Zhou, F. Zhao, et al., ACS Nano 13 (2019) 7913–7919.
[61] L. Wu, Z.C. Dong, Z.R. Cai, et al., Nat. Commun. 11 (2020) 521.
[62] S.J. Cao, A. Thomas, C. Li, Angew. Chem. Int. Ed. 62 (2023) e202214391.
[63] X.Y. Li, K.L. Yang, Z.Q. Yuan, et al., Chem. Rec. 23 (2023) e202200298.
[64] X. Huang, J.Z. Liu, P. Zhou, et al., Small 18 (2022) 2104048.
[65] L.T. Ren, X.L. Yi, Z.S. Yang, et al., Nano Lett 21 (2021) 1709–1715.
[66] H. Xie, Y. Du, W.L. Zhou, et al., Small 19 (2023) 2300915.
[67] D.H. Wang, Q.Q. Sun, M.J. Hokkanen, et al., Nature 582 (2020) 55–59.
[68] Y.Y. Zhou, H.L. Chen, Nano 13 (2018) 1850005.
[69] J.C. Gomez-Vidal, NPJ Mater. Degrad. 1 (2017) 1–9.
[70] L.B. Kong, Y.J. Li, X.F. Kong, et al., Compos. B. Eng. 232 (2022) 109588.
[71] S.Y. Pan, M. Chen, L.M. Wu, ACS Appl. Mater. Interfaces 12 (2020) 5157–5165.
[72] Y.H. Cai, D.Y. Chen, N.J. Li, et al., Langmuir 35 (2019) 13950–13957.
[73] M.C. Wu, Y. Li, N. An, et al., Adv. Funct. Mater. 26 (2016) 6777–6784.
[74] X.T. Han, L.L. Ren, Y. Ma, et al., Carbon 197 (2022) 27–39.
[75] D.W. Li, L.J. Ma, B. Zhang, et al., Chen, Chem. Eng. J. 450 (2022) 138429.